Diagn Interv Radiol 2026; DOI: 10.4274/dir.2026.264368

MUSCULOSKELETAL IMAGING

ORIGINAL ARTICLE

©Copyright 2026 Author(s) - Available online at dirjournal.org.
Content of this journal is licensed under a Creative Commons Attribution-NonCommercial 4.0 International License.

Virtual non-calcium dual-energy computed tomography for postoperative lumbar spine evaluation following pedicle screw instrumentation

Muhammet Fırat Öztepe[1]
Tunç Batuhan Acar[1]
Volkan Kızılgöz[1]
Macit Terzi[2]
Ozan Kucukatalay[2]
Mecit Kantarci[1]

[1]Erzincan Binali Yıldırım University Faculty of Medicine, Department of Radiology, Erzincan, Türkiye

[2]Erzincan Binali Yıldırım University Faculty of Medicine, Department of Neurosurgery, Erzincan, Türkiye

PURPOSE

To compare standard grayscale CT, 140-keV virtual monoenergetic imaging, and virtual non-calcium (VNCa) for detection of magnetic resonance imaging (MRI)-defined relevant foraminal stenosis, disc protrusion or extrusion, and relevant nerve root compression.

METHODS

This retrospective study included patients who underwent dual-energy computed tomography (DECT) on a 128-slice single-tube system and MRI within 1 week between August and December 2025; CT reconstructions were read in consensus. Foraminal stenosis and nerve root compression grades 2–3 were considered imaging-defined relevant findings. Only segments with an MRI confidence score of 5 were included. Diagnostic performance and CT confidence scores were summarized descriptively.

RESULTS

Twenty-three patients (mean age, 60 ± 12 years; 15 women) contributed 185 evaluated segments. MRI showed relevant foraminal stenosis in 26 segments and disc protrusion or extrusion and relevant nerve root compression in 18 segments each. Foraminal-stenosis sensitivity was 100.0% (26/26) for VNCa and 92.3% (24/26) for both comparators; specificity was 88.7%, 71.1%, and 72.3% for VNCa, standard CT, and 140-keV CT, respectively. Disc protrusion or extrusion sensitivity was 77.8% (14/18) for VNCa and 11.1% (2/18) for both comparators. Standard CT and VNCa each had 83.3% sensitivity and 97.0% specificity for nerve root compression.

CONCLUSION

In this small, selected cohort, VNCa had higher observed specificity for MRI-defined foraminal stenosis and higher observed sensitivity for disc protrusion or extrusion. These exploratory findings require confirmation in larger studies that account for patient-level clustering and include more artifact-limited examinations.

CLINICAL SIGNIFICANCE

VNCa reconstruction from an existing DECT examination may complement grayscale CT for evaluating MRI-defined foraminal stenosis and disc protrusion or extrusion following lumbar pedicle screw instrumentation without requiring additional scanning.

KEYWORDS

Dual-energy computed tomography, foraminal stenosis, lumbar spine, pedicle screw instrumentation, virtual noncalcium imaging

Handling editor: Elif Günay Bulut

Corresponding author: Muhammet Fırat Öztepe

E-mail: firatoztepe92@gmail.com

Received 11 August 2026; revision requested 09 September 2026; last revision requested 24 October 2026; accepted 31 October 2026.

Epub: 13.11.2026

DOI: 10.4274/dir.2026.264368

You may cite this article as: Öztepe MF, Acar TB, Kızılgöz V, Terzi M, Kucukatalay O, Kantarci M. Virtual non-calcium dual-energy computed tomography for postoperative lumbar spine evaluation following pedicle screw instrumentation. *Diagn Interv Radiol*. 13 November 2026 DOI: 10.4274/dir.2026.264368 [Epub Ahead of Print].

Lumbar fusion with pedicle screw instrumentation is performed to restore stability and alleviate symptoms in selected patients with degenerative disease, deformity, or pseudoarthrosis.[1,2] Recurrent disc herniation and adjacent segment degeneration may contribute to new or recurrent postoperative symptoms.[3,4]

Magnetic resonance imaging (MRI) is the primary modality for evaluating postoperative disc and neural abnormalities, but susceptibility artifacts near metallic implants can obscure the operative field.[2] High-bandwidth acquisition, short tau inversion recovery fat suppression, and dedicated techniques such as slice encoding for metal artifact correction and multiacquisition variable-resonance image combination can mitigate these limitations.[5,6] Computed tomography (CT) is frequently used to assess implant position and fusion and may also be required when MRI is contraindicated or unavailable.

Dual-energy CT (DECT) provides reconstructions with different potential contributions; virtual non-calcium (VNCa) imaging uses material decomposition to enhance the display of non-calcium tissues and has shown promise for lumbar disc assessment.[7] High-energy virtual monoenergetic imaging (VMI) can reduce some implant-related artifacts.[8,9] Improved soft-tissue contrast and reduced metal artifacts are distinct effects; a diagnostic benefit from VNCa cannot be attributed to artifact reduction without directly evaluating that mechanism.

Most previous DECT studies in instrumented spines have emphasized technical image quality or artifact reduction, leaving limited evidence on detection of disc herniation, foraminal stenosis, and nerve root compression using MRI as the reference standard.[8,10-13] We therefore compare standard grayscale CT, 140-keV VMI, and VNCa for these imaging-defined outcomes following lumbar pedicle screw instrumentation.

Main points

- The study included 23 patients with 185 evaluated segments; the observations do not represent 185 independent patients.
- Virtual non-calcium (VNCa) imaging had higher observed specificity for imaging-defined relevant foraminal stenosis and higher observed sensitivity for disc protrusion or extrusion than the two grayscale computed tomography (CT) reconstructions.
- Standard CT and VNCa had identical aggregate sensitivity and specificity estimates for imaging-defined relevant nerve root compression. Higher diagnostic confidence did not establish higher diagnostic accuracy.

Methods

Study design and patient selection

This retrospective, single-center study was approved by the Erzincan Binali Yıldırım University Faculty of Medicine Review Board (decision/protocol number: 2026-08/01; date: April 30, 2026), which waived written informed consent. Patients who underwent both DECT and MRI for routine postoperative evaluation between August and December 2025 were retrospectively identified. Twenty-eight patients were initially assessed. After the segment-level exclusions, 5 patients had no eligible segments remaining, resulting in a final cohort of 23 patients and 185 segments. The median interval between CT and MRI was 2 days [interquartile range (IQR), 0–4 days; range, 0–7 days]. The median number of instrumented levels per patient was 4 (IQR, 4–5; range, 2–5), with a mean of 4.2 ± 0.8. All instrumentation procedures were performed at our institution.

Segments containing interbody cages or crosslinks were excluded to reduce heterogeneity in implant configuration and its potential effect on visualization of adjacent disc and neural structures. Segments with an MRI diagnostic confidence score below 5 were excluded to establish a high-confidence imaging reference. This selection restricted the analysis to cases in which MRI remained fully interpretable.

Computed tomography acquisition and reconstruction

Dual-energy CT was performed as part of the routine clinical postoperative lumbar spine imaging protocol. Non-contrast CT was performed using a 128-slice single-tube dual-energy system (SOMATOM go.Top; Siemens Healthineers, Forchheim, Germany). Acquisition parameters were 100/Sn140 kV, a rotation time of 0.50 seconds, and a pitch of 0.80. Three image sets were generated using syngo.via: standard grayscale mixed CT (blending ratio, 0.6), 140-keV VMI, and VNCa. Reconstruction settings were SAFIRE level 3, a QR40 kernel, and a 1.5-mm section thickness. The tube-voltage pair and reconstruction settings were consistent across patients, whereas tube current was automatically modulated according to patient attenuation.

High-energy VMI has been investigated for reduction of implant-related artifacts;[8-13] 140 keV was the only monoenergetic level assessed in this study. Its inclusion does not establish that 140 keV is optimal for postoperative soft-tissue evaluation. All three reconstructions for each patient originated from the same DECT examination, and generating the additional reconstructions did not require additional scanning. No dedicated CT metal artifact reduction (MAR) reconstruction was included as a comparator.

VNCa images were generated via three-material decomposition using previously reported lumbar disc settings: low-energy color chart, spectrum; high-energy color chart, grayscale; and CT preset 1, liver;[7] VNCa was assessed as a color-coded display, whereas mixed CT and 140-keV VMI were assessed in grayscale. Accordingly, the comparison included differences in visual presentation and reconstruction type.

Magnetic resonance image acquisition

MRI was performed without contrast material at 1.5 T (MAGNETOM Aera; Siemens Healthineers, Erlangen, Germany) using a dedicated spine coil. The protocol included sagittal T2-weighted (T2W) turbo spin-echo [repetition time (TR)/echo time (TE), 3,620/120 ms], sagittal T1W turbo spin-echo (TR/TE, 599/6.7 ms), and axial T2W turbo spin-echo (TR/TE, 4,430/96 ms) imaging, each with a 4-mm section thickness. MAR was applied to all MRI sequences.

Image analysis and reference standard

All CT and MRI datasets were anonymized before review. Two radiologists with 10 and 20 years of experience (M.F.Ö and V.K.) evaluated the CT datasets in consensus while blinded to clinical information and MRI findings. Mixed CT, 140-keV CT, and VNCa were reviewed in separate sessions. The interval between sessions was not prospectively standardized or recorded, and the order of the reconstruction types was not randomized. Disagreements were resolved by joint re-evaluation; unresolved disagreements were independently adjudicated by a third radiologist with 29 years of experience (M.K.). Final consensus or adjudicated scores were analyzed.

The same two radiologists evaluated the MRI examinations in consensus as the imaging reference while blinded to the CT findings. All imaging sequences (sagittal T2W, sagittal T1W, and axial T2W) were used for all diagnostic assessments. Disagreements were resolved by joint re-evaluation, with unresolved disagreements independently

adjudicated by the same third radiologist. A 5-point scale was used for diagnostic confidence, ranging from 1 (non-diagnostic image quality) to 5 (complete diagnostic confidence).[7,14] Only segments with an MRI confidence score of 5 were included in diagnostic performance analyses.

The unit of analysis was a level-side observation, with the right and left sides of each lumbar intervertebral level evaluated separately. Foraminal stenosis, disc pathology, and nerve root compromise were assessed independently for each side, with disc abnormalities classified according to their location and extension on the corresponding side. Foraminal stenosis was graded from 0 to 3 on sagittal images using the Lee system, which considers perineural fat obliteration and nerve root morphology.[15] Nerve root compromise was graded using the Pfirrmann classification (0, no compromise; 1, contact; 2, deviation; 3, compression).[16] Disc morphology was classified as absent, bulging, protrusion, or extrusion according to lumbar disc nomenclature recommendations; no sequestered discs were present.[17]

For binary analyses, grades 2–3 were considered positive for foraminal stenosis and nerve root involvement, whereas disc protrusion or extrusion was considered a positive disc finding. Thus, nerve root involvement included both grade 2 deviation and grade 3 compression. These thresholds were based solely on imaging findings, without clinical or surgical correlation.

Statistical analysis

This was an exploratory study of a fixed retrospective cohort, and no a priori sample size calculation was performed. Patient-level characteristics and the number of evaluated segments are reported separately. Sensitivity, specificity, positive predictive value, negative predictive value, and accuracy were calculated from the MRI-referenced classification counts. The 95% confidence intervals (CIs) were calculated using the Wilson score method. These intervals are unadjusted segment-level binomial summaries and do not account for correlation among segments from the same patient.

Between-reconstruction findings are presented descriptively, without confirmatory *P* values; CT diagnostic confidence scores are summarized as mean ± standard deviation, with no inferential comparison that treats all segments as independent; MRI confidence was not compared statistically with CT because a score of 5 was required for inclusion. Diagnostic confidence and diagnostic accuracy were considered separate outcomes.

Results

Study population

Twenty-eight patients were initially assessed. After exclusion of 24 segments containing interbody cages or crosslinks and 30 segments with MRI confidence scores below 5, five patients had no eligible segments remaining. The final cohort comprised 23 patients (mean age, 60 ± 12 years; range, 30–75 years), including 15 women and eight men, with 185 evaluated segments. Patient characteristics and the distribution of evaluated levels are summarized in Table 1, the selection process is shown in Figure 1, and patient- and level-specific exclusions are detailed in Supplementary Table 1.

Among the 23 included patients, the median CT dose index was 19.4 mGy (range, 16.6–32.8 mGy), and the median dose–length product was 683 mGy·cm (range, 603–1,175 mGy·cm).

Table 1. Patient characteristics and evaluated lumbar levels

Characteristic	Value
Patients	23
Age in years	60 ± 12 (30–75)
Women	15 (65.2)
Age of women in years	64 ± 10 (44–75)
Men	8 (34.8)
Age of men in years	53 ± 14 (30–70)
Evaluated segments	185
L1–2	24 (13.0)
L2–3	40 (21.6)
L3–4	46 (24.9)
L4–5	42 (22.7)
L5–S1	33 (17.8)

Data are mean ± SD (range) or number (%). The cohort contains 23 patients; level percentages use the 185 evaluated segments as their denominator. SD, standard deviation.

Diagnostic performance

MRI showed relevant foraminal stenosis in 26/185 segments (14.1%) and disc protrusion or extrusion and relevant nerve root compression in 18/185 segments (9.7%) each. Diagnostic performance estimates and unadjusted 95% CIs are presented in Table 2.

For foraminal stenosis, VNCa detected all 26 MRI-positive segments, whereas standard CT and 140-keV CT each detected 24. The observed sensitivity difference was therefore 7.7 percentage points, corresponding to two additional detections per comparison. Moreover, VNCa yielded 18 false-positive classifi-

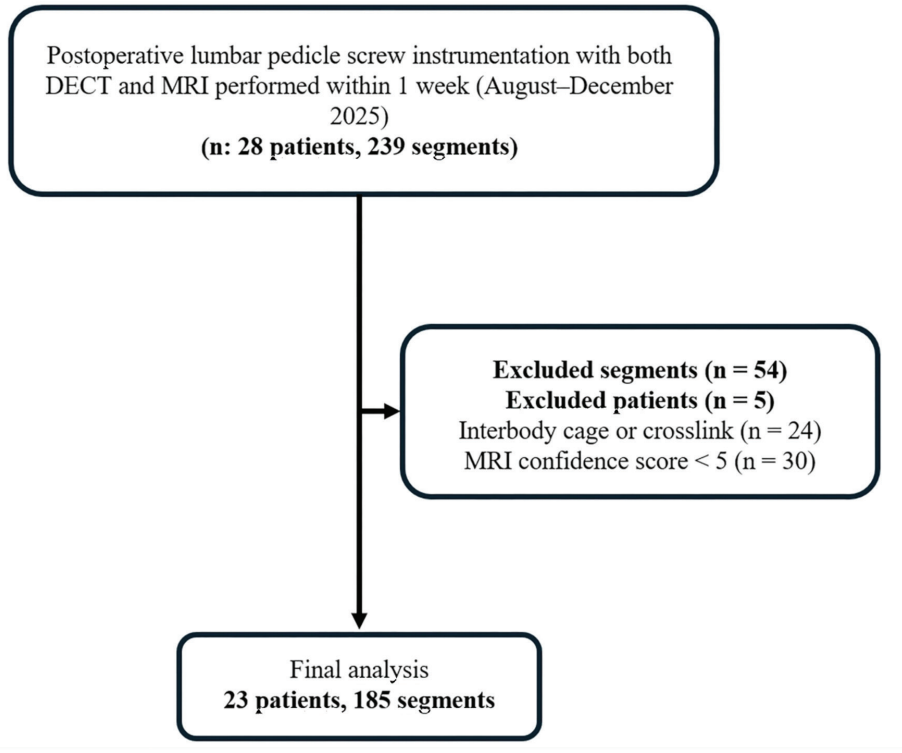


Figure 1. Flowchart of patient and segment selection. DECT, dual-energy computed tomography; MRI, magnetic resonance imaging.

Table 2. Magnetic resonance imaging-referenced diagnostic performance

Outcome and method	Sensitivity % (95% CI)	Specificity % (95% CI)	PPV % (95% CI)	NPV % (95% CI)	Accuracy % (95% CI)
Foraminal stenosis					
Standard CT	92.3 (75.9–97.9)	71.1 (63.6–77.6)	34.3 (24.2–46.0)	98.3 (93.9–99.5)	74.1 (67.3–79.8)
140-keV CT	92.3 (75.9–97.9)	72.3 (64.9–78.7)	35.3 (25.0–47.2)	98.3 (94.0–99.5)	75.1 (68.4–80.8)
VNCa	100.0 (87.1–100.0)	88.7 (82.8–92.7)	59.1 (44.4–72.3)	100.0 (97.3–100.0)	90.3 (85.1–93.8)
Disc protrusion or extrusion					
Standard CT	11.1 (3.1–32.8)	96.4 (92.4–98.3)	25.0 (7.1–59.1)	91.0 (85.8–94.4)	88.1 (82.7–92.0)
140-keV CT	11.1 (3.1–32.8)	96.4 (92.4–98.3)	25.0 (7.1–59.1)	91.0 (85.8–94.4)	88.1 (82.7–92.0)
VNCa	77.8 (54.8–91.0)	98.8 (95.7–99.7)	87.5 (64.0–96.5)	97.6 (94.1–99.1)	96.8 (93.1–98.5)
Nerve root compression					
Standard CT	83.3 (60.8–94.2)	97.0 (93.2–98.7)	75.0 (53.1–88.8)	98.2 (94.8–99.4)	95.7 (91.7–97.8)
140-keV CT	77.8 (54.8–91.0)	97.0 (93.2–98.7)	73.7 (51.2–88.2)	97.6 (94.0–99.1)	95.1 (91.0–97.4)
VNCa	83.3 (60.8–94.2)	97.0 (93.2–98.7)	75.0 (53.1–88.8)	98.2 (94.8–99.4)	95.7 (91.7–97.8)

Data are percentages (unadjusted 95% Wilson CIs); MRI-positive/negative counts were 26/159 for foraminal stenosis and 18/167 for both disc protrusion or extrusion and nerve root compression. Positive thresholds were grade ≥ 2 for foraminal stenosis and nerve root compression, and protrusion or extrusion for the disc endpoint. The CIs do not account for patient-level clustering and are descriptive. PPV, positive predictive value; NPV, negative predictive value; CT, computed tomography; VNCa, virtual non-calcium imaging; CI, confidence interval; MRI, magnetic resonance imaging.

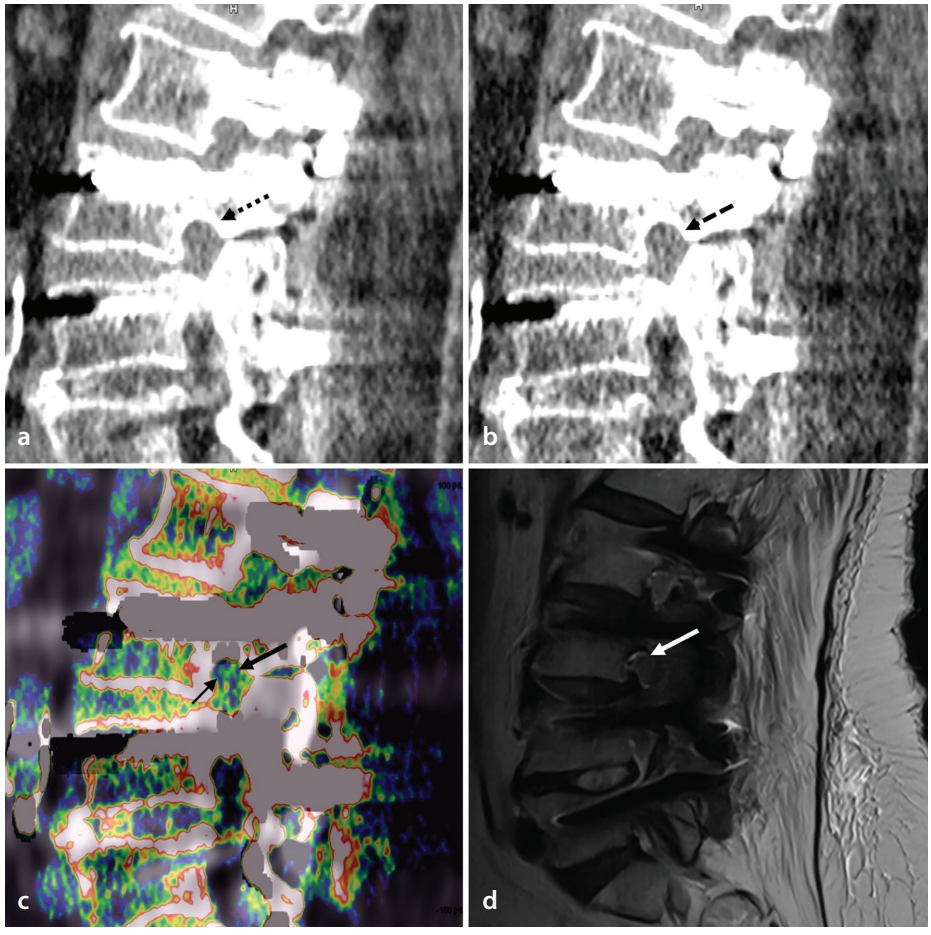


Figure 2. A 75-year-old woman with grade 1 foraminal stenosis. **(a, b)** Sagittal non-contrast standard computed tomography (CT) and 140-keV CT, respectively, show poor delineation of perineural fat and overestimate stenosis as grade 2 (dotted and dashed arrows, respectively). **(c)** Color-coded virtual non-calcium imaging shows the nerve root and adjacent perineural fat in contrasting colors (solid black arrows), supporting a grade 1 classification. **(d)** The sagittal T2-weighted magnetic resonance reference image confirms grade 1 stenosis (white arrow). This case illustrates correction of a false-positive classification at the grade ≥ 2 threshold.

cations, compared with 46 for standard CT and 44 for 140-keV CT. Figure 2 illustrates a grade 1 foramen overcalled as grade 2 on the grayscale CT reconstructions and correctly classified below the positive threshold on VNCa.

For disc protrusion or extrusion, VNCa detected 14/18 MRI-positive segments (77.8%), whereas both grayscale reconstructions detected 2/18 (11.1%); VNCa yielded 2 false-positive classifications, compared with 6 for each grayscale reconstruction. Figure 3 illustrates an extrusion visible on all reconstructions, with greater conspicuity on VNCa; this example illustrates confidence in an already detected lesion.

For relevant nerve root compression, standard CT and VNCa each identified 15/18 MRI-positive segments (83.3%), whereas 140-keV CT identified 14/18 (77.8%). All three reconstructions yielded 5 false-positive classifications. Identical aggregate estimates for standard CT and VNCa do not establish equivalence or show that the same individual segments were correctly classified. Figure 4 illustrates MRI-defined nerve root compression not clearly depicted by any CT reconstruction.

Diagnostic confidence

Mean CT diagnostic confidence scores were numerically highest for VNCa for all three outcomes (Table 3). The mean VNCa score was 4.01 for foraminal stenosis, 4.20 for disc pathology, and 3.40 for nerve root compression. These descriptive confidence findings do not establish a corresponding

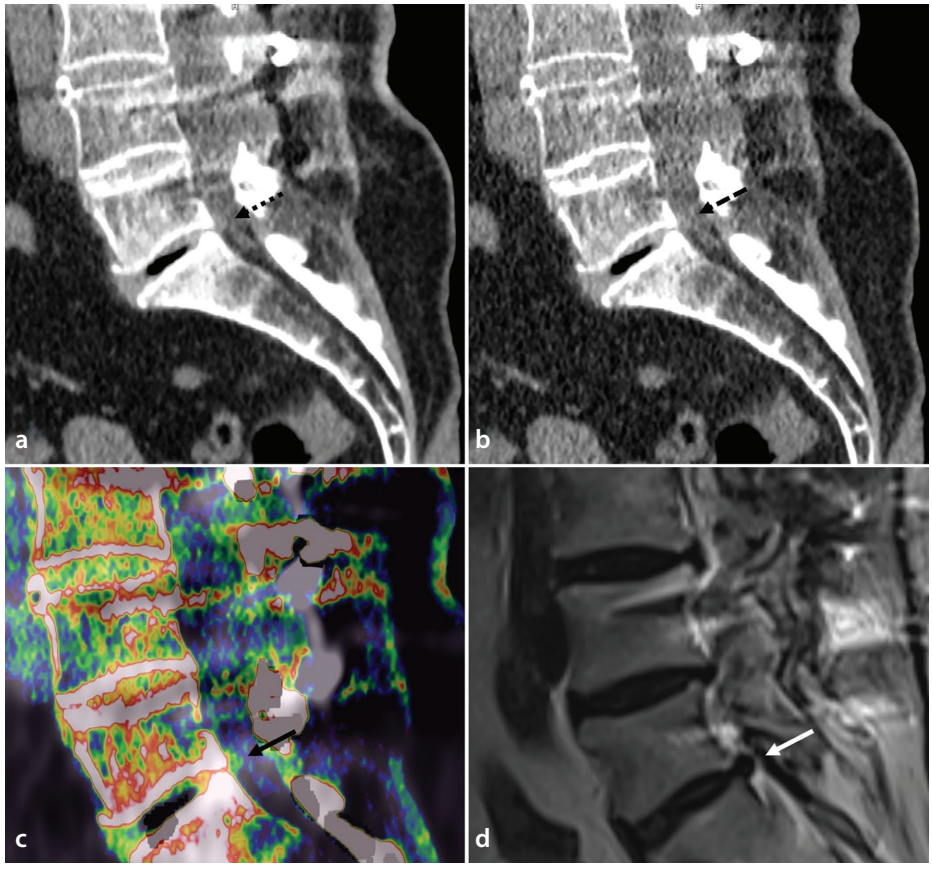


Figure 3. A 66-year-old man with lumbar disc extrusion. **(a, b)** Sagittal non-contrast standard computed tomography (CT) and 140-keV CT, respectively, show the extrusion with limited delineation of its margins (dotted and dashed arrows). **(c)** Color-coded sagittal virtual non-calcium (VNCa) imaging depicts the extrusion more conspicuously (solid black arrow). **(d)** The sagittal T2-weighted magnetic resonance reference image confirms the extrusion (white arrow). The lesion is visible on all reconstructions; the example illustrates a difference in conspicuity rather than an additional VNCa detection.

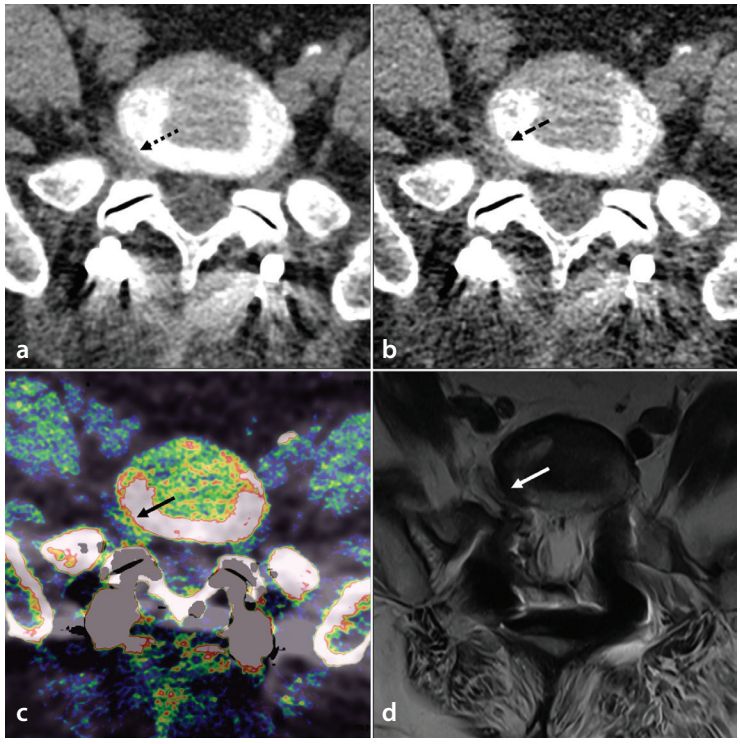


Figure 4. A 75-year-old woman with right-sided nerve root compression. **(a–c)** Axial non-contrast standard computed tomography (CT), 140-keV CT, and color-coded virtual non-calcium imaging, respectively, do not clearly delineate the right foraminal disc protrusion or its relationship to the adjacent nerve root (dotted, dashed, and solid black arrows). **(d)** The axial T2-weighted magnetic resonance reference image shows the right foraminal protrusion and marked nerve root compression, classified as grade 3 (white arrow).

Table 3. Descriptive computed tomography diagnostic confidence

Outcome	Standard CT	140-keV CT	VNCa
Foraminal stenosis	2.10 ± 0.61	1.90 ± 0.42	4.01 ± 0.54
Disc pathology	2.30 ± 0.64	2.17 ± 0.58	4.20 ± 0.60
Nerve root compression	1.80 ± 0.40	1.60 ± 0.49	3.40 ± 0.66

Data are mean ± SD on a 5-point scale. These summaries are descriptive; they do not account for the dependence of multiple observations from the same patient. Magnetic resonance imaging (MRI) confidence was 5 by the inclusion criterion and is omitted. No Friedman, Wilcoxon, or MRI-vs.-CT *P* values are reported. SD, standard deviation; CT, computed tomography; VNCa, virtual non-calcium imaging.

increase in diagnostic accuracy; MRI confidence was 5 by the inclusion criterion and was excluded from the comparative confidence table.

Discussion

In this exploratory cohort of 23 patients, VNCa showed higher observed specificity for MRI-defined foraminal stenosis and higher observed sensitivity for disc protrusion or extrusion than standard CT and 140-keV CT. The foraminal-stenosis sensitivity difference represented only two additional positive segments. Standard CT and VNCa had identical aggregate diagnostic estimates for relevant nerve root compression. The results should be interpreted as descriptive findings in a selected population, not evidence of general diagnostic superiority.

The observed disc findings are consistent in direction with previous studies of lumbar VNCa, including the DECT study by Booz et al.[7] and the photon-counting CT study by Shu et al.[18] Differences in patient selection, instrumentation, reference standards, and reconstruction settings preclude direct comparison of performance estimates across studies. Our data do not determine which of these factors accounts for differences from earlier reports.

Improved display of disc material and perineural tissues is a plausible explanation for the observed VNCa findings. Specifically, the lower false-positive count for foraminal stenosis may reflect easier distinction of preserved perineural fat from adjacent neural or degenerative tissue. However, artifact magnitude and tissue contrast were not quantified. Furthermore, VNCa was displayed in color whereas the comparators were grayscale. The respective contributions of material decomposition, color presentation, and artifact behavior therefore cannot be separated. Higher reader confidence does not demonstrate this mechanism or independently validate diagnostic accuracy.

The findings at 140 keV should not be generalized to all VMI energies or dedicated MAR methods. High-energy VMI can reduce beam-hardening artifacts, but increasing keV may also reduce tissue contrast, and the optimal energy level may depend on the imaging platform and diagnostic task. Previous studies of spinal instrumentation have investigated VMI and MAR using different platforms and technical endpoints.[8,10-13] Additional approaches include combined VMI and iterative MAR (IMAR) in split-filter DECT and tin prefiltration in low-dose CT.[19,20] More recently, a photon-counting CT angiography study in patients with knee arthroplasty demonstrated marked differences in artifact reduction and diagnostic assessability among seven IMAR presets, further emphasizing the importance of task- and anatomy-specific optimization.[21] However, these findings cannot be directly extrapolated to lumbar soft-tissue assessment. Because our study evaluated only 140-keV VMI and did not include a dedicated MAR reconstruction, it cannot determine the optimal monoenergetic energy or the potential additional benefit of dedicated MAR.

Photon-counting CT offers a further platform for spectral reconstruction and has been investigated for lumbar VNCa imaging.[18] Patzer et al.[22] evaluated VMI combined with IMAR in patients with dental implants. That study provides a technical rationale for evaluating complementary reconstruction strategies, but its dental setting does not establish diagnostic benefit in the postoperative lumbar spine. Future instrumented-spine studies should compare VNCa, multiple VMI energies, and dedicated MAR using both artifact measurements and clinically interpretable diagnostic endpoints.

This study has several limitations. First, the retrospective single-center cohort included only 23 patients and 26, 18, and 18 MRI-positive segments for the three endpoints. Multiple segments from the same patient are correlated and do not increase the independent patient sample size. Consequently, sensitivity estimates, particularly the observed 100% foraminal-stenosis sensitivity, are uncertain. Furthermore, the reported Wilson intervals are not adjusted for patient clustering, and confidence scores are descriptive. No adjusted analysis of age or segment level was included, although these characteristics may influence image quality and diagnostic performance. Moreover, requiring an MRI confidence score of 5 may have introduced selection bias by excluding technically difficult segments. Therefore, diagnostic performance may be overestimated, and the findings may not be generalizable to patients with suboptimal postoperative MRI, marked spinal deformity, or advanced degenerative changes. Additionally, exclusion of interbody cages and crosslinks further limits applicability to more complex postoperative constructs.

Consensus interpretation precluded estimation of interreader agreement from the analyzed consensus scores. Because the interval between CT reading sessions was not prospectively standardized or recorded and the reconstruction order was not randomized, repeated evaluation of the same anatomy may have introduced recall bias. In addition, the endpoints were imaging defined; the analysis did not establish associations with symptoms, operative findings, or clinical outcomes.

Finally, the study used a single CT vendor, one implant material, one high-keV reconstruction, and specific VNCa settings. No dedicated MAR comparator, grayscale VNCa comparison, or quantitative assessment of artifact reduction was included. Generalization to other scanners, implant configurations, reconstruction algorithms, or display settings requires separate validation.

In this small, selected cohort, VNCa showed higher observed specificity for MRI-defined foraminal stenosis and higher observed sensitivity for disc protrusion or extrusion than standard CT and 140-keV CT. The findings support further evaluation of VNCa as a complementary reconstruction from an existing DECT examination. They do not establish performance in MRI-nondiagnostic cases or a clinical outcome benefit.

Footnotes

Conflict of interest disclosure

The authors declared no conflicts of interest.

Supplementary Table Link: https://d2v96fxpocvxx.cloudfront.net/68f48462-babf-415b-b878-1e392d1c83af/content-images/eee82d9e-1798-4d0a-a687-22322a8ba9f4.pdf

References

1. Reid PC, Morr S, Kaiser MG. State of the union: a review of lumbar fusion indications and techniques for degenerative spine disease. *J Neurosurg Spine.* 2019;31(1):1-14. [Crossref]
2. Abel F, Tan ET, Chazen JL, Lebl DR, Sneag DB. MRI after lumbar spine decompression and fusion surgery: technical considerations, expected findings, and complications. *Radiology*. 2023;308(1):e222732. [Crossref]
3. McGirt MJ, Ambrossi GL, Datoo G, et al. Recurrent disc herniation and long-term back pain after primary lumbar discectomy: review of outcomes reported for limited versus aggressive disc removal. *Neurosurgery*. 2009;64(2):338-344; discussion 344-355. [Crossref]
4. Zhang C, Berven SH, Fortin M, Weber MH. Adjacent segment degeneration versus disease after lumbar spine fusion for degenerative pathology: a systematic review with meta-analysis of the literature. *Clin Spine Surg*. 2016;29(1):21-29. [Crossref]
5. Feuerriegel GC, Sutter R. Managing hardware-related metal artifacts in MRI: current and evolving techniques. *Skeletal Radiol*. 2024;53(9):1737-1750. [Crossref]
6. Ulbrich EJ, Sutter R, Aguiar RF, Nittka M, Pfirrmann CW. STIR sequence with increased receiver bandwidth of the inversion pulse for reduction of metallic artifacts. *AJR Am J Roentgenol.* 2012;199(6):W735-W742. [Crossref]
7. Booz C, Nöske J, Martin SS, et al. Virtual noncalcium dual-energy CT: detection of lumbar disk herniation in comparison with standard gray-scale CT. *Radiology*. 2019;290(2):446-455. [Crossref]
8. Popp D, Sinzinger AX, Decker JA, et al. Spectral metal artifact reduction after posterior spinal fixation in photon-counting detector CT datasets. *Eur J Radiol.* 2023;165:110946. [Crossref]
9. Bamberg F, Dierks A, Nikolaou K, Reiser MF, Becker CR, Johnson TR. Metal artifact reduction by dual energy computed tomography using monoenergetic extrapolation. *Eur Radiol.* 2011;21(7):1424-1429. [Crossref]
10. Dangelmaier J, Schwaiger BJ, Gersing AS, et al. Dual layer computed tomography: reduction of metal artefacts from posterior spinal fusion using virtual monoenergetic imaging. *Eur J Radiol.* 2018;105:195-203. [Crossref]
11. Long Z, DeLone DR, Kotsenas AL, et al. Clinical assessment of metal artifact reduction methods in dual-energy CT examinations of instrumented spines. *AJR Am J Roentgenol.* 2019;212(2):395-401. [Crossref]
12. Große Hokamp N, Neuhaus V, Abdullayev N, et al. Reduction of artifacts caused by orthopedic hardware in the spine in spectral detector CT examinations using virtual monoenergetic image reconstructions and metal-artifact-reduction algorithms. *Skeletal Radiol.* 2018;47(2):195-201. [Crossref]
13. Ceccarelli L, Vara G, Ponti F, et al. Reduction of metal artifacts caused by titanium peduncular screws in the spine by means of monoenergetic images and the metal artifact reduction software in dual-energy computed tomography. *J Med Phys.* 2022;47:152-158. [Crossref]
14. Notohamiprodjo S, Stahl R, Braunagel M, et al. Diagnostic accuracy of contemporary multidetector computed tomography (MDCT) for the detection of lumbar disc herniation. *Eur Radiol.* 2017;27(8):3443-3451. [Crossref]
15. Lee S, Lee JW, Yeom JS, et al. A practical MRI grading system for lumbar foraminal stenosis. *AJR Am J Roentgenol.* 2010;194(4):1095-1098. [Crossref]
16. Pfirrmann CW, Dora C, Schmid MR, Zanetti M, Hodler J, Boos N. MR image-based grading of lumbar nerve root compromise due to disk herniation: reliability study with surgical correlation. *Radiology.* 2004;230(2):583-588. [Crossref]
17. Fardon DF, Williams AL, Dohring EJ, Murtagh FR, Gabriel Rothman SL, Sze GK. Lumbar disc nomenclature: version 2.0: recommendations of the combined task forces of the North American Spine Society, the American Society of Spine Radiology and the American Society of Neuroradiology. *Spine J.* 2014;14(11):2525-2545. [Crossref]
18. Shu D, Zhang C, Wang J, et al. Detection of lumbar disc herniation and degeneration using photon-counting detector CT with virtual non-calcium imaging. *Eur Radiol.* 2026;36(2):1319-1329. [Crossref]
19. Schmidt AMA, Grunz JP, Petritsch B, et al. Combination of iterative metal artifact reduction and virtual monoenergetic reconstruction using split-filter dual-energy CT in patients with dental artifact on head and neck CT. *AJR Am J Roentgenol.* 2022;218(4):716-727. [Crossref]
20. Huflage H, Grunz JP, Hackenbroch C, et al. Metal artefact reduction in low-dose computed tomography: benefits of tin prefiltration versus postprocessing of dual-energy datasets over conventional CT imaging. *Radiography (Lond).* 2022;28(3):690-696. [Crossref]
21. Huflage H, Kunz AS, Wech T, et al. Comparison of iterative metal artifact reduction presets in ultra-high-resolution photon-counting CT angiography of patients with total knee endoprosthesis. *Acad Radiol.* 2026;33(9):4136-4143. [Crossref]
22. Patzer TS, Kunz AS, Huflage H, et al. Combining virtual monoenergetic imaging and iterative metal artifact reduction in first-generation photon-counting computed tomography of patients with dental implants. *Eur Radiol.* 2023;33(11):7818-7829. [Crossref]